RSC Advances

PAPER

View Article Online
View Journal | View Issue

Cite this: *RSC Adv.*, 2026, **16**, 20559

A sustainable spectrofluorimetric method for ivabradine quantification based on erythrosin B quenching with quantum mechanical modeling and Box–Behnken design optimization

Arwa Sultan Alqahtani,[a] Maram H. Abduljabbar,[b] Reem M. Alnemari,[c] Musaad M. Althobaiti,[b] Mohammed F. Aldawsari,[d] Aamal A. Al-Mutairi,[a] Ahmed Serag *[e] and Atiah H. Almalki[fg]

A novel, sensitive, and environmentally sustainable spectrofluorimetric method was developed for ivabradine determination based on the fluorescence quenching of erythrosin B. The method exploits the formation of a stable 1 : 1 ground-state complex between anionic erythrosin B and cationic ivabradine through electrostatic interactions. To elucidate the interaction mechanism, comprehensive mechanistic studies using Stern–Volmer analysis, thermodynamic parameters determination, and Job's method confirmed static quenching with spontaneous complex formation. Furthermore, quantum mechanical calculations using PM3 methodology revealed multiple interaction sites with binding distances of 1.7–3.6 Å, involving electrostatic interactions and hydrogen bonding. Subsequently, Box–Behnken experimental design optimization identified optimal conditions: pH 5.6, buffer volume 1.1 mL, erythrosin B concentration 25 μg mL^{-1}, and reaction time 4.0 minutes. Under these optimized conditions, the method demonstrated excellent analytical performance with linear response over 0.02–2.0 μg mL^{-1} (r^2 = 0.9995), superior sensitivity (LOD = 6.46 ng mL^{-1}), high accuracy, and precision. The practical applicability was demonstrated through successful application to commercial tablets and spiked human plasma samples, confirming utility for both pharmaceutical quality control and bioanalytical applications. Therefore, the developed method represents a significant advancement in green analytical chemistry, offering a cost-effective, rapid, and environmentally friendly alternative for ivabradine monitoring in pharmaceutical and clinical settings.

Received 28th January 2026
Accepted 31st March 2026

DOI: 10.1039/d6ra00744a

rsc.li/rsc-advances

1 Introduction

Ivabradine hydrochloride (IVB) is a cardiovascular therapeutic agent used in the treatment of heart failure and chronic stable angina pectoris.[1] As the first selective inhibitor of the hyperpolarization-activated cyclic nucleotide-gated (HCN) channels, ivabradine specifically targets the funny current (I_f) in sinoatrial nodal tissue, resulting in a dose-dependent reduction in heart rate without affecting cardiac contractility, blood pressure, or systemic vascular resistance.[2,3] This mechanism of action distinguishes ivabradine from conventional heart rate-lowering agents such as beta-blockers and calcium channel blockers.[4] The drug's selectivity is attributed to its ability to block specific ion channels in their open state, creating enhanced effectiveness at faster heart rates.[5] Clinical studies have demonstrated ivabradine's therapeutic efficacy, with trials showing significant reductions in cardiovascular events and hospital admissions for heart failure patients.[6,7] Additional research has confirmed ivabradine's effectiveness in treating chest pain and reducing exercise-induced symptoms, showing superior benefits compared to placebo and comparable efficacy to established medications like atenolol or amlodipine.[8–10] These clinical results led to regulatory approvals by the European Medicines Agency and the U.S. Food and Drug Administration.[1] Ivabradine undergoes extensive metabolism in the liver through the cytochrome P450 enzyme system, with therapeutic doses ranging from 2.5 to 7.5 mg administered twice daily.[1]

[a]*Department of Chemistry, College of Science, Imam Mohammad Ibn Saud Islamic University (IMSIU), P.O. Box 90950, Riyadh 11623, Saudi Arabia*
[b]*Department of Pharmacology and Toxicology, College of Pharmacy, Taif University, P.O. Box 11099, Taif 21944, Saudi Arabia*
[c]*Department of Pharmaceutics and Industrial Pharmacy, College of Pharmacy, Taif University, P.O. Box 11099, Taif 21944, Saudi Arabia*
[d]*Department of Pharmaceutics, College of Pharmacy, Prince Sattam Bin Abdulaziz University, Al-kharj 11942, Saudi Arabia*
[e]*Pharmaceutical Analytical Chemistry Department, Faculty of Pharmacy, Al-Azhar University, Nasr City 11751, Cairo, Egypt. E-mail: Ahmedserag777@hotmail.com*
[f]*Addiction and Neuroscience Research Unit, Health Science Campus, Taif University, P.O. Box 11099, Taif 21944, Saudi Arabia*
[g]*Department of Pharmaceutical Chemistry, College of Pharmacy, Taif University, P.O. Box 11099, Taif 21944, Saudi Arabia*

Given ivabradine's therapeutic importance and complex pharmacokinetic profile, precise analytical methods are essential for pharmaceutical quality control, bioanalytical studies, and therapeutic drug monitoring to ensure safe and effective treatment outcomes.

The analytical determination of ivabradine has been extensively investigated using chromatographic techniques, with high-performance liquid chromatography (HPLC) and liquid chromatography-tandem mass spectrometry (LC-MS/MS) representing the most widely employed approaches.[11–18] HPLC methods have utilized various stationary phases including C18 and C8 reversed-phase columns with diverse mobile phase compositions.[11,12] For instance, Rashad *et al.* developed a dual detection HPLC method using a HyperClone™ MOS C8 column with an ethanol:methanol:phosphate buffer mobile phase, achieving a linearity range of 0.50–16 μg mL^{-1} for ivabradine with a 5 minutes run time.[11] Similarly, Nowakowska *et al.* employed a Knauer C8 column with acetonitrile–ammonium acetate mobile phase, demonstrating dual wavelength detection at 207 nm and 286 nm with detection limits of 0.33–1.19 μg mL^{-1}.[14] However, HPLC methods present several analytical limitations including lengthy analysis times that can extend up to 13 minutes per sample, significantly reducing laboratory throughput and efficiency. The extensive use of organic solvents such as acetonitrile and methanol raises environmental concerns regarding chemical waste disposal and sustainability, particularly in high-throughput analytical laboratories. Moreover, UV detection systems employed in conventional HPLC methods demonstrate inherently limited sensitivity, with detection limits typically in the microgram per milliliter range, which may be insufficient for trace-level analysis in biological matrices or quality control applications requiring enhanced sensitivity.[12,13]

LC-MS/MS methods have emerged as highly sensitive techniques for ivabradine bioanalysis, offering exceptional specificity through multiple reaction monitoring.[15–18] For example, Lu *et al.* developed a method for simultaneous determination of ivabradine and its metabolite *N*-desmethylivabradine in human plasma and urine, achieving detection limits of 0.1013 ng mL^{-1} in plasma using a Diamonsil C18 column with methanol–ammonium acetate mobile phase.[17] Another study by Zoerner *et al.* reported a UPLC-MS/MS method with analysis times of 4.5 minutes using a Waters ACQUITY BEH C18 column, demonstrating a linearity range of 1–500 ng mL^{-1} for clinical trial applications.[18] Despite their analytical advantages, LC-MS/MS techniques require substantial capital investment and ongoing maintenance costs, making them inaccessible for many laboratories with limited budgets. The complexity of method development necessitates specialized training and expertise, while matrix effects and ion suppression can compromise analytical reliability, requiring extensive validation and quality control measures.[16]

Electrochemical methods have been explored as alternative approaches, with Abo-Talib *et al.* developing ion-selective electrodes using different ionophores, achieving linear ranges spanning 10^{-5} to 10^{-2} mol L^{-1}.[19] Abdel-Haleem *et al.* reported a molecularly imprinted polymer optode with a detection limit of 3.1 μM and response time of 1–2 minutes.[20] While electrochemical methods offer cost-effectiveness and simplicity, they suffer from limited selectivity in complex pharmaceutical matrices and biological samples, where interfering substances can significantly affect analytical accuracy.

Spectrofluorimetric methods have emerged as attractive alternatives offering significant advantages including enhanced sensitivity, cost-effectiveness, and environmental sustainability.[21,22] Fluorescence spectroscopy provides inherently superior sensitivity compared to UV detection, with the ability to achieve detection limits in the nanogram range due to the direct proportionality between fluorescence intensity and analyte concentration at low concentrations.[23] The technique requires minimal sample preparation, reduced solvent consumption, and offers rapid analysis times, making it an environmentally friendly approach for pharmaceutical analysis.[24,25] Several spectrofluorimetric methods have been developed for ivabradine analysis, exploiting the drug's intrinsic fluorescence properties in the UV-visible region. Native fluorescence methods utilizing excitation around 287 nm and emission at 325 nm have demonstrated linearity ranges of 100–500 ng mL^{-1} with detection limits ranging from 8.38 ng mL^{-1}.[26] To address spectral overlap issues in multi-component pharmaceutical formulations, synchronous fluorescence spectroscopy has been extensively employed with various wavelength differences ($\Delta\lambda$ = 20–80 nm), achieving enhanced selectivity and detection limits ranging from 3.07–4.88 ng mL^{-1} for ivabradine in combination with different cardiovascular drugs.[27–29] These methods have successfully demonstrated applicability in pharmaceutical dosage forms and human urine samples. However, existing spectrofluorimetric methods face significant analytical challenges that limit their practical applications. The reliance on UV excitation wavelengths (280–290 nm) poses substantial interference problems due to the strong autofluorescence of biological matrices, proteins, and excipients commonly found in pharmaceutical formulations, which can severely compromise analytical accuracy and precision.[27–29] Additionally, UV excitation increases the risk of photodegradation of the analyte during measurement, potentially affecting method reliability. These limitations highlight the need for alternative fluorescence approaches which can minimize matrix interference, reduce photodegradation risks, and provide enhanced selectivity for ivabradine determination in complex pharmaceutical and biological matrices.

Fluorescent probes have emerged as powerful analytical tools in pharmaceutical analysis, offering exceptional sensitivity and selectivity for drug determination.[30,31] These probes function through various mechanisms including fluorescence enhancement, quenching, or energy transfer, enabling detection limits in the nanogram to picogram range.[32,33] The advantages of fluorescent probe-based methods include rapid analysis times, minimal sample preparation, cost-effectiveness, and environmental friendliness due to reduced organic solvent consumption.[34] Erythrosin B, a xanthene-based fluorescent dye, has gained particular attention as an analytical probe due to its excellent photophysical properties, including high quantum yield, good photostability, and strong fluorescence emission

with excitation in the visible region.[35] Its operation in the far-red spectral region offers significant analytical advantages by minimizing interference from biological autofluorescence, protein fluorescence, and matrix components that typically emit in the UV-blue region. The probe's ability to form stable ground-state complexes with drug molecules makes it particularly suitable for developing sensitive, selective, and environmentally friendly analytical methods for pharmaceutical quality control applications.[36,37]

Therefore, the primary objective of this research is to develop and validate a novel, sensitive, and environmentally sustainable spectrofluorimetric method for ivabradine determination based on the fluorescence quenching of erythrosin B. The specific objectives are: (1) comprehensive characterization of the spectral properties of ivabradine and investigation of its interaction mechanism with erythrosin B through UV-visible absorption and fluorescence spectroscopy; (2) elucidation of the quenching mechanism using Stern–Volmer kinetic analysis, thermodynamic parameters determination, and Job's method for stoichiometric evaluation; (3) quantum mechanical calculations employing semi-empirical PM3 methodology to determine binding energy, interaction sites, and molecular properties of the formed complex; (4) systematic optimization of critical experimental factors including pH, buffer volume, erythrosin B concentration, and reaction time using Box–Behnken design to maximize analytical performance; (5) rigorous validation of the developed method according to ICH Q2(R2) guidelines,[38] evaluating linearity, sensitivity, accuracy, precision, robustness, and selectivity; (6) application of the method to pharmaceutical formulations and spiked human plasma samples to demonstrate practical applicability; and (7) comprehensive greenness, blueness, and whiteness assessments using Analytical Greenness (AGREE), Blue Applicability Grade Index (BAGI), and Red–Green–Blue 12 (RGB12) tools to evaluate the environmental impact, analytical practicality, and overall sustainability of the proposed methodology. This comprehensive approach aims to provide a robust, sustainable, and clinically relevant analytical solution for ivabradine monitoring in pharmaceutical quality control and therapeutic drug monitoring applications.

2 Experimental

2.1 Materials and reagents

Ivabradine hydrochloride reference standard (purity 99.5%) was kindly supplied by the Egyptian Drug Authority (EDA, Cairo, Egypt). Erythrosin B fluorescent dye (dye content ≥95%) was procured from Sigma-Aldrich (St. Louis, MO, USA). HPLC-grade acetonitrile was also obtained from Sigma-Aldrich (St. Louis, MO, USA) for sample preparation and extraction processes. Analytical grade chemicals including boric acid, phosphoric acid, acetic acid, and sodium hydroxide required for Britton–Robinson buffer preparation were purchased from El-Nasr Pharmaceutical Chemicals Company (Cairo, Egypt). Commercial ivabradine hydrochloride tablets were acquired from local community pharmacies in Cairo, Egypt, for pharmaceutical formulation analysis. Drug-free human plasma samples for bioanalytical method validation were purchased VACSERA Blood Bank (Giza, Egypt), maintained at −20 °C during storage, and equilibrated to ambient temperature before experimental use.

Ivabradine hydrochloride stock solution (100 μg mL^{-1}) was prepared by accurately weighing 10 mg of the reference standard, transferring to a 100 mL volumetric flask, dissolving completely in distilled water under gentle stirring, and diluting to the mark. Working standard solutions covering the concentration range 0.02–2.0 μg mL^{-1} were freshly prepared daily through serial dilution of the stock solution using distilled water to ensure concentration accuracy for calibration and validation experiments. Erythrosin B stock solution (0.01% w/v) was prepared by accurately weighing 10 mg of the dye, transferring to a 100 mL volumetric flask, dissolving completely in distilled water under gentle stirring, and diluting to the mark. The solution was preserved in amber glassware, protected from direct light exposure, and demonstrated stability for at least two weeks when stored at 4 °C. Britton–Robinson buffer solutions spanning the pH range 3.0–8.0 were prepared by combining appropriate volumes of a mixed acid solution containing 0.04 M each of boric acid, phosphoric acid, and acetic acid, followed by precise pH adjustment to desired values using 0.2 M sodium hydroxide solution with continuous monitoring using a calibrated pH meter.

2.2 Instrumentation

Fluorescence spectroscopic measurements were carried out using a Jasco FP-6200 spectrofluorometer (Jasco International Co., Ltd, Tokyo, Japan) including a 150 W xenon arc lamp as excitation source and equipped with standard 1 cm path length quartz cuvettes. The instrument parameters were optimized with excitation and emission slit widths maintained at 5 nm to ensure maximum signal-to-noise ratio, while the spectral scanning rate was adjusted to 4000 nm min^{-1} for rapid data acquisition. Spectral data collection and fluorescence intensity quantification at the analytical wavelengths of 528 nm (excitation) and 555 nm (emission) were accomplished using Spectra Manager software (version 1.53). Ultraviolet-visible absorption measurements were obtained using a Shimadzu UV-1800 dual-beam spectrophotometer (Shimadzu Corporation, Kyoto, Japan) incorporating matched 1 cm quartz cells and operated through UV Probe software (version 2.43). Spectral acquisition parameters included a 1 nm spectral resolution with rapid scan mode over the 220–600 nm wavelength region for molecular interaction characterization. Solution pH determination and control were achieved using a Jenway 3510 digital pH meter (Jenway, Staffordshire, UK) following daily three-point calibration using certified reference buffers at pH 4.0, 7.0, and 10.0.

2.3 Optimization of experimental conditions

A four-factor, three-level Box–Behnken design was employed to systematically optimize the experimental conditions affecting the fluorescence quenching interaction between erythrosin B and ivabradine hydrochloride. The independent variables selected for optimization were pH (Factor A), Britton–Robinson buffer volume (Factor B, mL), erythrosin B concentration (Factor C, μg mL^{-1}), and reaction time (Factor D, minutes). The

experimental ranges were established as pH 3.0–8.0, buffer volume 0.5–1.5 mL, erythrosin B concentration 10–30 μg mL^{-1}, and reaction time 3.0–10.0 minutes based on preliminary univariate studies and practical analytical considerations. The Box–Behnken design matrix generated 29 experimental runs including factorial points, axial points, and center point replications distributed throughout the experimental domain to ensure comprehensive factor space coverage (Table S1). All experiments were conducted in randomized order to minimize systematic errors and temporal variations. Box–Behnken design experimental runs were performed as single measurements as per standard response surface methodology practice, with center points replicated five times (runs 11, 16, 19, 22, and 23, corresponding to standard order 27, 25, 26, 28, and 29 at fixed conditions of pH 5.5, buffer volume 1.0 mL, erythrosin B concentration 20 μg mL^{-1}, and reaction time 6.5 min) to provide an independent estimate of pure experimental error for model validation and lack-of-fit assessment purposes.

The fluorescence quenching efficiency (QE%) was selected as the response variable for optimization, calculated using the equation:

$$QE\% = [(F_0 - F)/F_0] \times 100$$

where F_0 represents the fluorescence intensity of erythrosin B alone, and F represents the fluorescence intensity after ivabradine addition at a fixed concentration of 1.0 μg mL^{-1}. A quadratic polynomial model was fitted to the experimental data using Design Expert® software (version 11.1.2.0) to establish the relationship between the response and independent variables. Model adequacy and significance were evaluated through analysis of variance (ANOVA) with F-test at 95% confidence level ($p < 0.05$). Model quality parameters including coefficient of determination (R^2), adjusted R^2, predicted R^2, and adequate precision were calculated to assess predictive capability. Non-significant model terms were eliminated through backward regression analysis to obtain the final optimized model. Response surface methodology was applied to identify optimal experimental conditions that maximize fluorescence quenching efficiency while ensuring analytical robustness and practical implementation for routine analysis.

2.4 General analytical procedure

The optimized analytical procedure for ivabradine determination using erythrosin B fluorescence quenching was performed as follows: into a series of 10 mL volumetric flasks, 1.1 mL of Britton–Robinson buffer (pH 5.6) and appropriate volumes of ivabradine standard solution or sample solution were added to achieve final concentrations within the linear range of 0.02–2.0 μg mL^{-1}. Subsequently, 2.5 mL of erythrosin B stock solution (0.01% w/v) was added to each flask to obtain a final reagent concentration of approximately 25 μg mL^{-1}. The solutions were mixed thoroughly by gentle swirling and allowed to stand for 4.0 minutes at ambient temperature (25 ± 2 °C) to ensure complete interaction between the fluorescent probe and ivabradine molecules. The reaction mixtures were then diluted to volume with distilled water and mixed again.

Fluorescence measurements were conducted immediately after dilution using the optimized instrumental parameters of 528 nm excitation wavelength and 555 nm emission wavelength with 1 cm quartz cuvettes. A blank solution containing all reagents except ivabradine was prepared under identical conditions, and its fluorescence intensity (F_0) was recorded. The fluorescence intensity (F) of each standard or sample solution was measured under the same experimental conditions. Calibration curves were constructed by plotting ivabradine concentration *versus* the fluorescence intensity ratio (F_0/F). All fluorescence measurements were performed in triplicate ($n = 3$), and results are expressed as mean ± standard deviation.

2.5 Quantum mechanical calculations

Molecular modeling studies were conducted using the Gaussian 09 computational chemistry software (Gaussian Inc., Wallingford, CT, USA) to elucidate the binding interactions between ivabradine and erythrosin B molecules. The initial three-dimensional structures of ivabradine, erythrosin B, and their potential binding complex were constructed and visualized using GaussView 6.0 molecular graphics interface. Complete geometry optimization was performed employing the semi-empirical PM3 computational method, which offers a balanced approach between computational efficiency and accuracy for large organic molecular systems containing multiple aromatic rings and heteroatoms.

The interaction energy between ivabradine and erythrosin B was determined using the computational equation:

$$\Delta E = E(\text{complex}) - E(\text{ivabradine}) - E(\text{erythrosin B})$$

where E(complex), E(ivabradine), and E(erythrosin B) correspond to the total electronic energies of the optimized complex structure, individual ivabradine molecule, and individual erythrosin B molecule, respectively. Negative ΔE values indicate energetically favorable complex formation with thermodynamically stable binding interactions.

Complementary molecular descriptors including dipole moments and molecular polarizability were computed to characterize the electronic properties and intermolecular forces governing the association process. The calculations were executed under standard computational conditions in the gas phase to ensure reproducibility and enable systematic comparison of the calculated molecular parameters. Convergence criteria were set to default Gaussian 09 values with tight optimization thresholds to ensure accurate energy minimization and reliable molecular property predictions. The optimized geometric parameters and calculated energetic data were subsequently used to support the experimental fluorescence quenching mechanism and validate the proposed molecular interaction model.

2.6 Applications to real samples

2.6.1 Analysis of pharmaceutical formulations. Commercial Procoralan 5 mg tablets (containing ivabradine) were analyzed using the developed fluorescence quenching method.

Ten tablets were accurately weighed to determine the average tablet weight, then pulverized to a homogeneous fine powder using a clean mortar and pestle. A portion of the powdered sample equivalent to 10 mg ivabradine was accurately transferred to a 100 mL volumetric flask and dissolved in approximately 30 mL of distilled water with the assistance of ultrasonication for 15 minutes to ensure complete drug extraction from the tablet matrix. The resulting solution was filtered through Whatman No. 42 filter paper to remove insoluble excipients and tablet debris, and the clear filtrate was diluted to volume with distilled water to obtain a stock solution containing 100 μg mL^{-1} ivabradine. Working solutions within the analytical range were prepared by appropriate serial dilution with distilled water and subjected to analysis following the general analytical procedure described in Section 2.4. Blank tablet matrix solutions were prepared using the same extraction procedure without drug addition to account for potential fluorescence interference from pharmaceutical excipients.

2.6.2 Analysis of spiked human plasma samples. Human plasma samples were fortified with known amounts of ivabradine to evaluate the method's performance in biological matrices. Plasma samples were spiked to achieve final concentrations of 0.025, 0.05, 1.0, and 1.5 μg mL^{-1} during the analytical procedure. For sample preparation, 5 mL of each spiked plasma sample was transferred to a clean centrifuge tube and treated with 15 mL of acetonitrile for protein precipitation. The mixture was vortexed vigorously for 2 minutes and centrifuged at 5000 rpm for 10 minutes at 4 °C to separate precipitated proteins. The clear supernatant was carefully collected and evaporated to dryness under a gentle nitrogen stream at 40 °C. The dried residue was reconstituted with 1 mL of distilled water, vortexed for 1 minute, and filtered through a 0.22 μm syringe filter before analysis. The reconstituted samples were analyzed according to the optimized procedure, with drug-free plasma samples processed identically to subtract background interference. Recovery studies were performed using matrix-matched calibration curves prepared by spiking blank plasma samples with known concentrations of ivabradine and processed under identical conditions.

3 Results and discussion

3.1 Spectral characterization and photophysical properties

The UV-visible absorption spectra of erythrosin B, ivabradine, and their interaction complex recorded in triplicate ($n = 3$) at 25 ± 2 °C provided fundamental evidence for the photophysical properties and molecular interactions between the fluorescent probe and the analyte molecule (Fig. 1A). Erythrosin B exhibited a characteristic intense absorption maximum at 525 nm, which is attributed to the π–π* electronic transition of the extended conjugated xanthene chromophore system containing the tricyclic aromatic framework (Fig. S1). The drug ivabradine displayed a weaker absorption band with maximum at 286 nm, corresponding to the benzofuran moiety and its conjugated benzazepine ring system that provides the chromophoric properties of the molecule (Fig. S1). Upon interaction between erythrosin B and ivabradine, significant spectral changes were observed in the resulting absorption spectrum. The complex exhibited a hypsochromic shift of the erythrosin B absorption maximum from 525 nm to approximately 520 nm, accompanied by a notable hypochromic effect characterized by reduced absorbance intensity compared to the individual erythrosin B spectrum. These spectral alterations indicate ground-state complex formation between the anionic xanthene dye and cationic ivabradine molecule, resulting in perturbation of the electronic distribution within the chromophoric systems.

The fluorescence spectroscopic investigation revealed the photophysical behavior of the erythrosin B-ivabradine system (Fig. 1B). Erythrosin B demonstrated strong fluorescence emission with a maximum at 555 nm when excited at 528 nm, exhibiting a Stokes shift of 27 nm that is characteristic of xanthene-based fluorophores. The excitation spectrum showed optimal excitation efficiency at 528 nm, which corresponds well with the visible region absorption characteristics observed in the UV-visible studies. The systematic fluorescence quenching behavior upon incremental addition of ivabradine is clearly demonstrated in Fig. 1C, where progressive decrease in emission intensity at 555 nm was observed with increasing analyte concentration from 0 to 2.0 μg mL^{-1}, with all measurements performed in triplicate ($n = 3$) showing %RSD < 1.5% across all concentration levels. The preservation of emission spectral shape throughout the quenching process, along with the absence of new emission bands, suggests the formation of non-fluorescent ground-state complexes between the fluorescent probe and analyte without significant structural perturbation of the erythrosin B chromophore system.

3.2 Fluorescence quenching mechanism and thermodynamic studies

The fluorescence quenching of erythrosin B by ivabradine was systematically investigated to elucidate the underlying molecular interaction mechanism and establish the thermodynamic basis for analytical method development. Fluorescence quenching mechanisms can be broadly classified into several categories including inner filter effects, Förster resonance energy transfer (FRET), dynamic (collisional) quenching, and static (complex formation) quenching, each exhibiting distinct spectroscopic signatures and temperature dependencies. The inner filter effect was initially excluded as a potential quenching mechanism based on the UV-visible absorption data presented in Fig. 1A, which demonstrated minimal spectral overlap between the ivabradine absorption band ($\lambda_{max} = 286$ nm) and the erythrosin B excitation wavelength (528 nm), thereby eliminating significant light absorption competition that would otherwise reduce the effective excitation intensity. Similarly, FRET was systematically ruled out due to the insufficient overlap between the erythrosin B emission spectrum ($\lambda_{max} = 555$ nm) and the ivabradine absorption spectrum, as FRET requires substantial spectral overlap between donor emission and acceptor absorption profiles for efficient dipole–dipole energy transfer to occur over the typical 1–10 nm distance range.

Consequently, the investigation focused on distinguishing between dynamic (collisional) and static (complex formation)

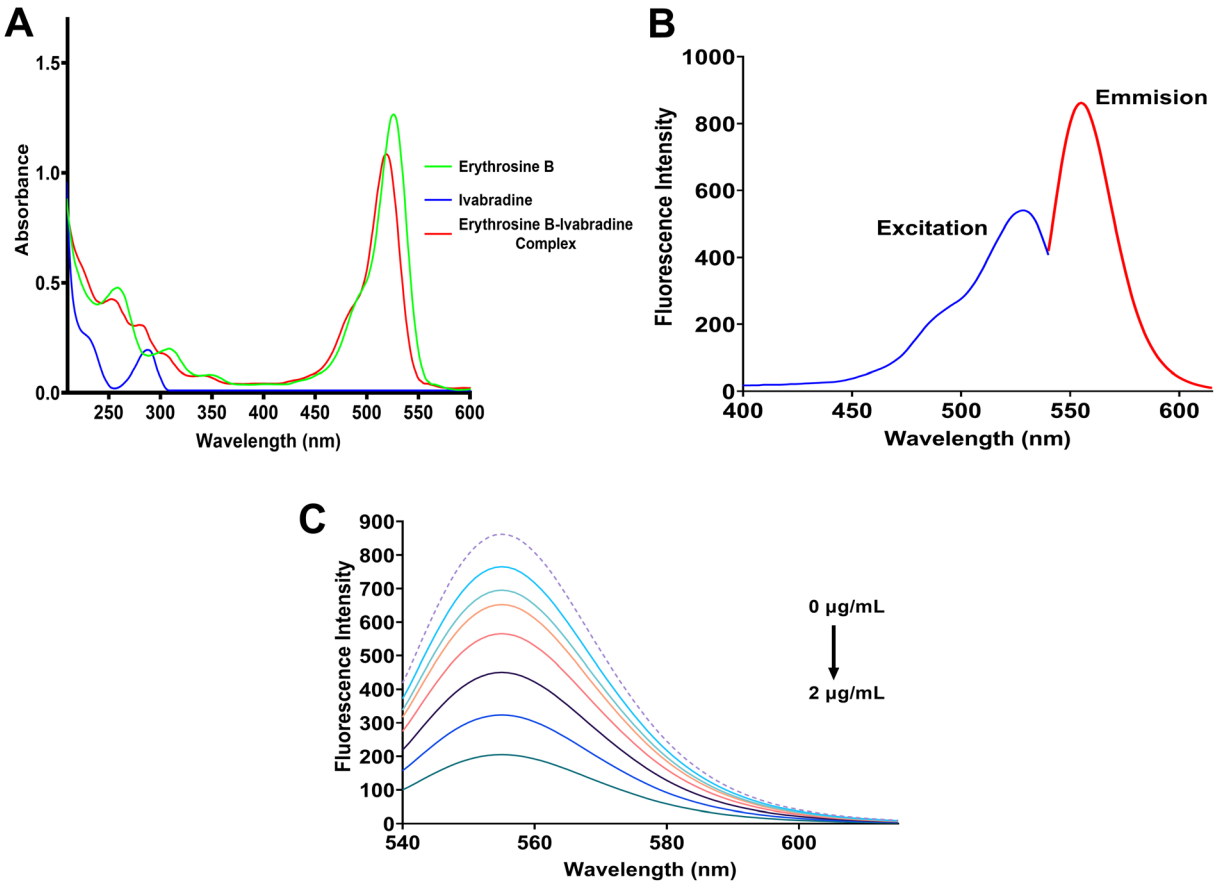

Fig. 1 Spectral characterization of the erythrosin B-ivabradine interaction system: (A) UV-visible absorption spectra of erythrosin B (25 µg mL^{-1}, green), ivabradine (1.0 µg mL^{-1}, blue), and their complex (red) in Britton–Robinson buffer (pH 5.6), showing hypsochromic shift and hypochromic effect upon complex formation; (B) fluorescence excitation (blue, $\lambda_{em} = 555$ nm) and emission (red, $\lambda_{ex} = 528$ nm) spectra of erythrosin B (25 µg mL^{-1}, pH 5.6) showing a Stokes shift of 27 nm; (C) progressive fluorescence quenching spectra upon incremental ivabradine addition (0–2.0 µg mL^{-1}, arrow indicates increasing concentration), showing systematic emission decrease with preserved spectral shape consistent with ground-state complex formation. All measurements in triplicate at 25 ± 2 °C.

quenching mechanisms through comprehensive temperature-dependent Stern–Volmer analysis, which provides the most reliable approach for mechanistic discrimination. The Stern–Volmer plots at three different temperatures (298, 303, and 313 K) are presented in Fig. 2A, showing excellent linear relationships between F_0/F and ivabradine concentration at all temperatures examined, with correlation coefficients exceeding 0.995 in all cases. Each data point represents the mean of triplicate measurements ($n = 3$), with standard deviation values yielding %RSD below 2.0% across all concentration levels and temperatures studied, confirming excellent measurement reproducibility. The calculated Stern–Volmer quenching constants (K_{sv}) were 7.13×10^5, 6.52×10^5, and 5.51×10^5 M^{-1} at 298, 303, and 313 K, respectively (Table 1). The observed systematic decrease in K_{sv} values with increasing temperature is characteristic of static quenching mechanisms, as elevated temperatures promote thermal dissociation of ground-state complexes and reduce the stability of intermolecular associations between fluorophore and quencher molecules. This temperature dependence contrasts sharply with dynamic quenching, where K_{sv} values typically increase with temperature due to enhanced molecular motion and collision frequency. To provide definitive confirmation of the static quenching mechanism, the bimolecular quenching rate constant (K_q) was calculated using the relationship $K_q = K_{sv}/\tau_0$, where τ_0 represents the intrinsic fluorescence lifetime of erythrosin B in the absence of quencher. Using the established fluorescence lifetime of erythrosin B ($\tau_0 \approx 0.8$ ns) reported in the literature for xanthene dyes in aqueous media,[39] the calculated K_q value at 298 K was approximately 8.91×10^{14} $M^{-1}s^{-1}$, which exceeds the theoretical maximum diffusion-controlled bimolecular quenching rate constant (approximately 10^{10} $M^{-1}s^{-1}$in aqueous solution at room temperature). This substantial four-order-of-magnitude deviation from diffusion-limited kinetics is a hallmark diagnostic criterion for static quenching, and has been similarly reported for other xanthene dye-drug systems including eosin Y-enalapril and erythrosin B-brexpiprazole complexes, where ion-pair formation between oppositely charged species constitutes the primary driving force for ground-state association.[21,35]

The association constants (K_a) were subsequently determined using the modified Stern–Volmer equation:

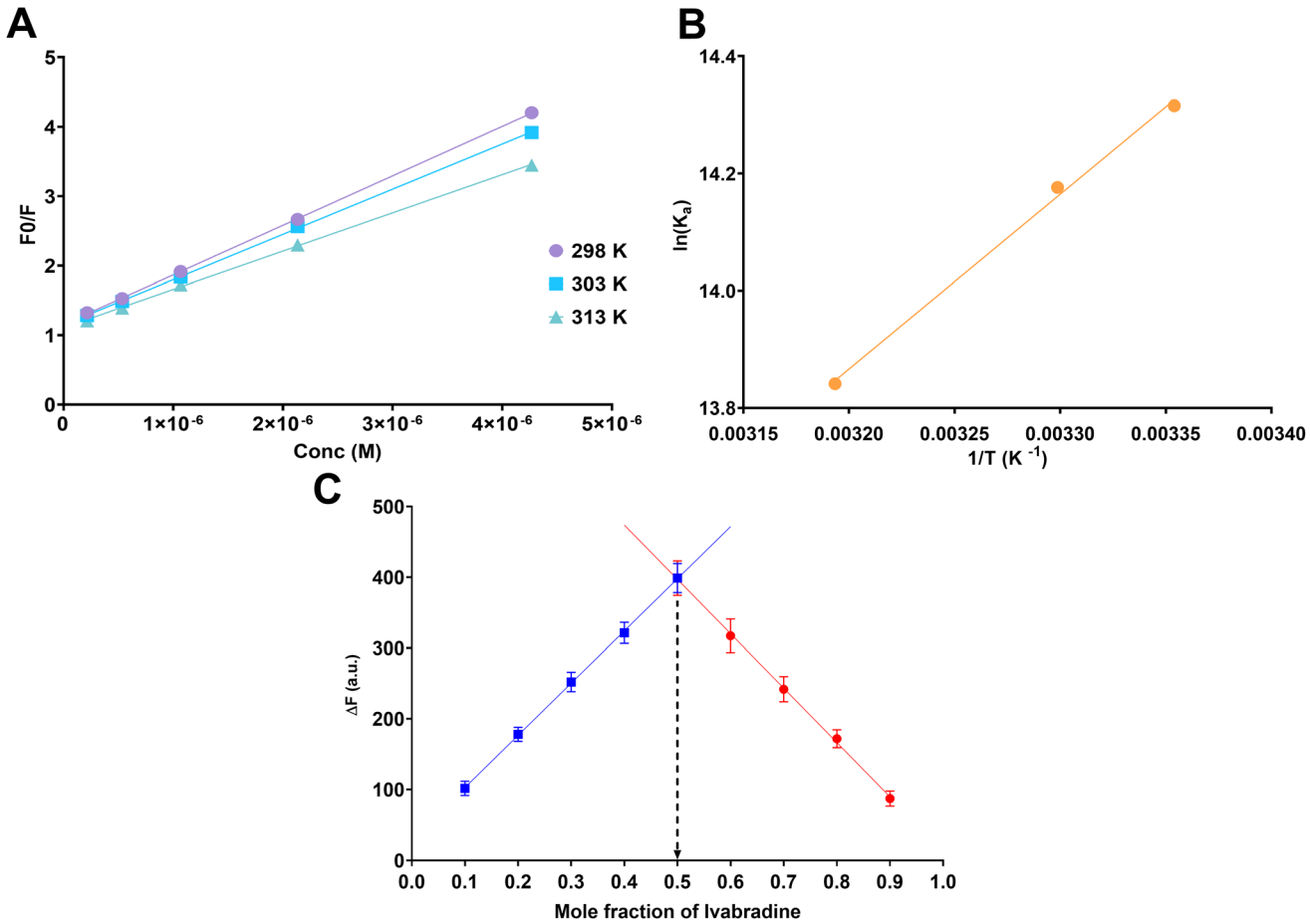

Fig. 2 Fluorescence quenching mechanism and thermodynamic studies of the erythrosin B-ivabradine system: (A) Stern–Volmer plots of F_0/F *versus* ivabradine molar concentration at 298 K (●), 303 K (■), and 313 K (▲) in Britton–Robinson buffer (pH 5.6); the decreasing K_{sv} values with increasing temperature confirm static quenching; error bars represent standard deviation of triplicate measurements; (B) Van't Hoff plot of ln(K_a) *versus* 1/T ($r^2 = 0.999$) yielding $\Delta H = -24.54$ kJ mol^{-1} and $\Delta S = 36.71$ J mol^{-1} K^{-1}, confirming spontaneous exothermic complex formation; (C) Job's method continuous variation plot of ΔF *versus* mole fraction of ivabradine (total concentration = 1.0 × 10^{-5} M, pH 5.6), with maximum at 0.5 confirming 1 : 1 binding stoichiometry.

Table 1 Thermodynamic parameters for erythrosin B-ivabradine interaction at different temperatures

Temperature (K)	K_{sv} (10^5 M^{-1})	K_a (10^6 M^{-1})	ΔG (kJ mol^{-1})	ΔH (kJ mol^{-1})	ΔS (J (mol^{-1} K^{-1}))
298	7.13	1.65	−35.49	−24.54	36.71
303	6.52	1.43	−35.73		
313	5.51	1.03	−36.04		

$$F_0/(F_0 - F) = 1/K_a[Q] + 1$$

where the double reciprocal plots yielded K_a values of 1.65 × 10^6, 1.43 × 10^6, and 1.03 × 10^6 M^{-1} at 298, 303, and 313 K, respectively (Table 1), demonstrating strong binding affinity between the interacting species. These K_a values are consistent with the range reported for similar xanthene dye-drug ion-pair complexes in the literature, where association constants typically fall within the 10^5–10^7 M^{-1} range, reflecting moderate-to-strong non-covalent binding that is analytically exploitable while remaining reversible under dilution conditions.[36,37] The comprehensive thermodynamic analysis revealed consistently negative Gibbs free energy changes (ΔG) at all temperatures studied (−35.49, −35.73, and −36.04 kJ mol^{-1} at 298, 303, and 313 K, respectively), confirming the thermodynamically spontaneous nature of complex formation and the high stability of the resulting ground-state association. The thermodynamic parameters governing the association process were calculated from the Van't Hoff plot (Fig. 2B), where ln(K_a) *versus* 1/T yielded an excellent linear relationship, providing a slope of $\Delta H/R$ and intercept of $\Delta S/R$ for thermodynamic parameter calculation. The derived enthalpy change (ΔH = −24.54 kJ mol^{-1}) and

entropy change ($\Delta S = 36.71$ J (mol^{-1} K^{-1})) indicated that the binding process is exothermic and entropy-driven, suggesting that favorable electrostatic interactions between oppositely charged species, complemented by hydrophobic interactions and desolvation effects, contribute synergistically to complex stabilization. According to the thermodynamic interaction classification proposed by Ross and Subramanian, negative ΔH and positive ΔS values are indicative of electrostatic interactions as the dominant binding force, which is fully consistent with the ion-pair formation mechanism proposed for the erythrosin B-ivabradine system. Furthermore, the stoichiometric composition of the erythrosin B-ivabradine complex was definitively established using Job's method of continuous variations, as illustrated in Fig. 2C. The characteristic plot of ΔF *versus* mole fraction of ivabradine exhibited a well-defined maximum at 0.5, unambiguously demonstrating a 1 : 1 binding stoichiometry between erythrosin B and ivabradine molecules, consistent with the formation of a simple binary complex through electrostatic attraction between the anionic xanthene framework and the cationic benzazepine moiety that serves as the analytical basis for sensitive ivabradine determination This 1 : 1 stoichiometry is in excellent agreement with previously reported xanthene dye-drug complexes, where the single carboxylate group of the xanthene framework typically engages with one protonated amine center of the drug molecule to form a simple binary ion-pair, as reported for similar systems including erythrosin B-raloxifene and eosin Y-enalapril complexes.[21,35]

3.3 Quantum mechanical calculations

The molecular interactions between erythrosin B and ivabradine were investigated using quantum mechanical calculations employing the semi-empirical PM3 method to provide theoretical support for the experimental findings and elucidate the binding mechanism at the molecular level. The PM3 method offers significant computational advantages for large molecular systems, including efficient calculation of molecular geometries, binding orientations, and relative energies with reasonable accuracy while maintaining manageable computational costs for complex drug-dye interactions. However, PM3 exhibits several well-documented inherent limitations that necessitate careful interpretation of the calculated energetic results. These include simplified parametrization that inadequately treats electron correlation effects, overestimation of electrostatic interactions in charged systems, and most importantly, the absence of solvent screening effects since all calculations were performed in the gas phase. The lack of explicit solvation modeling means that the calculated binding energy significantly overestimates the solution-phase interaction energy, as water molecules in the experimental system competitively solvate both the anionic carboxylate groups of erythrosin B and the cationic amine of ivabradine, thereby attenuating the net electrostatic attraction. This gas-phase overestimation of binding energies in PM3 calculations has been consistently noted in the literature for similar charged drug-dye systems and should be considered when comparing computational results with experimentally derived thermodynamic parameters. The computational analysis revealed significant changes in electronic properties upon complex formation, as summarized in Table 2. The individual erythrosin B molecule exhibited a total energy of −0.049215 Hartree with a dipole moment of 12.770417 Debye, reflecting its highly polar nature due to the presence of multiple charged centers including carboxylate groups and iodine substituents on the xanthene framework. The ivabradine molecule demonstrated a total energy of 0.057156 Hartree and a dipole moment of 10.168220 Debye, indicating significant polarity arising from the protonated tertiary amine group and the benzofuran–benzazepine framework. Upon complex formation, the optimized erythrosin B-ivabradine complex exhibited a total energy of −0.176216 Hartree, representing a substantial stabilization energy that confirms the thermodynamic favorability of the association process. The binding energy calculation yielded a value of −0.184157 Hartree, indicating strong intermolecular interactions driving complex formation. This calculated binding energy significantly exceeds the experimentally derived ΔG value of −35.49 kJ mol^{-1}, a discrepancy attributable to the combined effects of PM3 overestimation of electrostatic interactions in charged systems, the absence of solvent screening in gas-phase calculations, and the neglect of entropic contributions to the free energy in the total energy comparison. Similar discrepancies between PM3-calculated binding energies and experimentally determined thermodynamic parameters have been reported for analogous xanthene dye-drug systems and are considered an expected limitation of semi-empirical gas-phase modeling rather than an inconsistency in the experimental data. The complex formation resulted in a decrease in the dipole moment to 15.043089 Debye compared to the vector sum of individual dipole moments (22.938637 Debye), indicating charge neutralization and reorganization of electron density distribution upon ion-pair formation between the oppositely charged species (Table 2). Additionally, the molecular polarizability increased from individual values of 337.987667 and 247.564333 a.u. for erythrosin B and ivabradine, respectively, to 611.512057 a.u. for the complex, representing an increase of 25.960057 a.u. beyond the sum of individual polarizabilities, indicating enhanced electronic delocalization and intermolecular electronic interactions within the complex structure. This polarizability enhancement upon complexation is consistent with findings reported for other xanthene dye-drug systems and reflects the extended π-electron delocalization that occurs when the planar xanthene chromophore of erythrosin B interacts with the aromatic framework of ivabradine through combined electrostatic and π-stacking interactions. These computational results collectively demonstrate significant electronic reorganization upon complex formation, providing quantitative evidence for strong intermolecular binding that correlates well with the experimental thermodynamic and spectroscopic observations.

The optimized molecular structures of the individual components and their complex are presented in Fig. 3, where Fig. 3A shows the energy-minimized geometry of erythrosin B with its characteristic planar xanthene framework and peripheral iodine substituents that contribute to its high polarizability

Table 2 Quantum mechanical calculation results obtained using PM3 semi-empirical method, presenting total energies, charge distributions, dipole moments, and molecular polarizabilities for individual erythrosin B and ivabradine molecules and their optimized complex structure

Parameter	Erythrosin B	Ivabradine	Erythrosin B-ivabradine complex	Change (Δ)
Charge	−2	+1	−1	—
E(RPM3) (Hartree)	−0.049215	0.057156	−0.176216	−0.184157
RMS gradient norm (Hartree/Bohr)	0.000013	0.000002	0.000002	—
Dipole moment (Debye)	12.770417	10.168220	15.043089	−7.895548
Polarizability (α) (a.u.)	337.987667	247.564333	611.512057	+25.960057

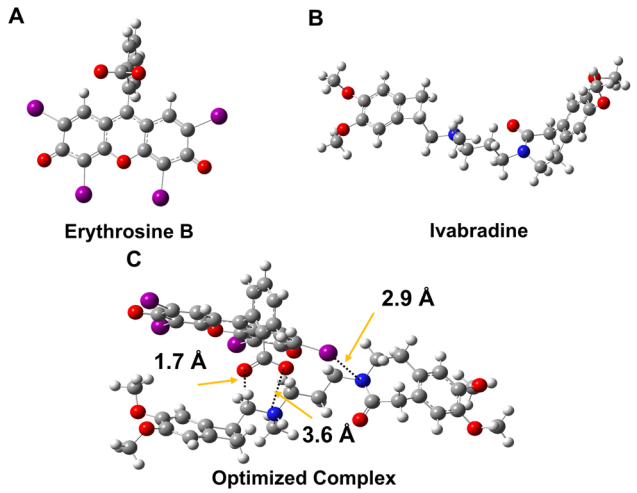

Fig. 3 Quantum mechanical calculations using PM3 semi-empirical methodology (Gaussian 09, gas phase): (A) energy-minimized structure of erythrosin B (E = −0.049215 Hartree, dipole = 12.77 Debye) showing the planar xanthene framework with peripheral iodine substituents and carboxylate groups; (B) optimized geometry of ivabradine (E = 0.057156 Hartree, dipole = 10.17 Debye) showing the benzofuran–benzazepine framework with protonated tertiary amine; (C) optimized complex geometry (ΔE = −0.184157 Hartree) showing three interaction sites: primary electrostatic ion-pair (3.6 Å), secondary electrostatic interaction involving iodine substituent (2.9 Å), and hydrogen bonding (1.7 Å). Calculations performed in gas phase; binding energies may be overestimated relative to solution-phase values due to absence of solvent screening effects.

and charge distribution. Fig. 3B illustrates the optimized structure of ivabradine, revealing the three-dimensional arrangement of the benzofuran–benzazepine framework with the protonated tertiary amine group positioned for optimal electrostatic interactions. The optimized complex geometry revealed multiple interaction sites that collectively contribute to the overall binding stability, as illustrated in Fig. 3C. The primary electrostatic interaction occurs between the protonated tertiary amine group of ivabradine and the carboxylate functionality of erythrosin B, with an intermolecular distance of 3.6 Å, indicating ion-pair formation between the positively charged nitrogen center and the negatively charged carboxyl oxygen that provides the dominant attractive force for complex stabilization. A secondary electrostatic interaction was identified between the amide group of ivabradine and one of the iodine substituents on the erythrosin B xanthene ring, separated by a distance of 2.9 Å. Furthermore, a hydrogen bonding interaction was observed between the carboxyl group of erythrosin B and a hydrogen atom on the CH_2 linker of the ivabradine tetracyclic framework, with an intermolecular distance of 1.7 Å, which falls within the range for strong hydrogen bonds and provides directional stabilization and contributes to the specific orientation of the molecules within the complex. The combination of these three distinct interaction modes – primary electrostatic ion-pairing, secondary electrostatic interaction involving the iodine substituent, and hydrogen bonding – creates a stable, multi-point binding arrangement that accounts for the high binding affinity observed experimentally and the 1 : 1 stoichiometry determined through Job's method. The identification of these specific binding sites and interaction distances provides molecular-level insight into the complex formation mechanism, validating the experimental evidence for static quenching and establishing a comprehensive understanding of the erythrosin B-ivabradine association that forms the analytical basis for sensitive fluorescence-based determination.

3.4 Optimization of experimental conditions

The optimization of experimental conditions for the erythrosin B-ivabradine fluorescence quenching system was systematically investigated using Box–Behnken design to establish the optimal parameter settings and understand the underlying factor interactions. Analysis of variance (ANOVA) results demonstrated the statistical significance and adequacy of the developed quadratic model for predicting fluorescence quenching efficiency (Table 3). The model exhibited high statistical significance with an F-value of 75.22 and p-value < 0.0001, indicating that the regression model effectively describes the relationship between the experimental factors and the response variable. Individual factor analysis revealed that pH (Factor A) and erythrosin B concentration (Factor C) were the most influential parameters, both showing p-values < 0.0001, while buffer volume (Factor B) demonstrated moderate significance. The interaction terms AB, AC, and BC all showed statistical significance (p < 0.05), confirming important synergistic effects between factors. The final regression model equation was established as: $QE\% = 70.18 + 8.59A + 4.05B + 9.04C - 4.15AB + 4.15AC + 10.53BC - 21.99A^2 - 16.32B^2 - 8.50C^2$, where the positive linear coefficients for pH, buffer volume, and reagent concentration indicate their favorable effects on quenching efficiency, while the negative quadratic terms confirm the curved response surfaces with optimal values rather than linear

Table 3 Analysis of variance (ANOVA) for Box–Behnken design optimization

Source	Sum of squares	df	Mean square	*F*-value	*p*-value	
Model	7105.80	9	789.53	75.22	<0.0001	Significant
A-pH	885.73	1	885.73	84.38	<0.0001	
B-buffer volume	197.03	1	197.03	18.77	0.0004	
C-reagent concentration	980.58	1	980.58	93.42	<0.0001	
AB	68.84	1	68.84	6.56	0.0191	
AC	68.89	1	68.89	6.56	0.0191	
BC	443.61	1	443.61	42.26	<0.0001	
A^2	3252.64	1	3252.64	309.87	<0.0001	
B^2	1791.82	1	1791.82	170.70	<0.0001	
C^2	485.60	1	485.60	46.26	<0.0001	
Residual	199.44	19	10.50			
Lack of fit	170.87	15	11.39	1.60	0.3494	Not significant
Pure error	28.57	4	7.14			
Cor total	7305.24	28				

relationships. The significant positive interaction coefficient *BC* (10.53) demonstrates strong synergy between buffer volume and reagent concentration, while the negative *AB* coefficient suggests competing effects between pH and buffer volume at extreme values.

Model validation parameters confirmed excellent model adequacy with $R^2 = 0.9727$, adjusted $R^2 = 0.9598$, and adequate precision of 29.25, indicating robust predictive capability (Table S2). Diagnostic plots (Fig. S2) showed normally distributed residuals with random scatter, confirming model assumptions and absence of systematic bias. The lack of fit test yielded non-significant results ($p = 0.3494$), validating that the model adequately represents the experimental data without major deviations.

Examination of individual factor effects (Fig. 4) provided mechanistic insights into the optimization process. The pH effect (Fig. 4A) showed a characteristic bell-shaped curve with optimal quenching efficiency around pH 5.6, which correlates with the ionization behavior of both interacting species. At this pH, erythrosin B exists predominantly in its anionic form, since its primary pK_a values are around 3.8 and 4.6, ensuring complete deprotonation of carboxyl groups for maximum electrostatic attraction with cationic ivabradine (p$K_a \approx 9.3$). Buffer volume effects (Fig. 4B) showed optimal performance around 1.1 mL, where ionic strength provides adequate electrolytic support without excessive dilution or ionic competition that disrupts electrostatic interactions. The erythrosin B concentration effect (Fig. 4C) demonstrated increasing efficiency up to approximately 20–25 μg mL^{-1} followed by plateauing, indicating saturation of available binding sites. Reaction time (Fig. 4D) exhibited minimal influence on quenching efficiency, with relatively flat response across the investigated range, suggesting rapid complex formation kinetics that reach equilibrium within the studied timeframe. The three-dimensional response surface plots and interaction effects (Fig. 5) revealed significant curvature and complex factor relationships. The pH-buffer volume interaction (Fig. 5A) demonstrated moderate curvature with the corresponding 3D surface (Fig. 5B) showing a broad optimal region. The pH-reagent concentration interaction (Fig. 5C) exhibited more pronounced curvature with the 3D plot (Fig. 5D) revealing a distinct maximum at intermediate pH values combined with higher reagent concentrations. The buffer volume-reagent concentration interaction (Fig. 5E) showed strong synergistic effects, with the 3D surface (Fig. 5F) displaying a sharp maximum, confirming the significant *BC* interaction coefficient in the regression model.

Response surface methodology and desirability function analysis identified optimal experimental conditions yielding maximum predicted quenching efficiency of 74.49%: pH 5.64, buffer volume 1.15 mL, erythrosin B concentration 25.34 μg mL^{-1}, and reaction time 3.91 minutes, as illustrated in the optimization ramp plots (Fig. S3). The overlay plots (Fig. S4) demonstrated the feasible optimization regions (yellow areas) where response criteria are simultaneously satisfied, providing operational flexibility while maintaining analytical performance. For practical implementation, these theoretical optimal values were rounded to experimentally feasible parameters: pH 5.6, buffer volume 1.1 mL, erythrosin B concentration 25 μg mL^{-1}, and reaction time 4.0 minutes. These optimized conditions were subsequently employed throughout the method validation studies and real sample analysis to ensure consistent analytical performance and reproducibility.

3.5 Method validation

The developed fluorescence quenching method was comprehensively validated according to ICH Q2(R2) guidelines to ensure its reliability and suitability for quantitative analysis of ivabradine.[38] The validation parameters are summarized in Table 4, demonstrating excellent analytical performance across all evaluated criteria. Linearity was established over the concentration range of 0.02–2.0 μg mL^{-1} using seven concentration levels with triplicate measurements at each level ($n = 21$ total measurements), yielding a linear regression equation with a slope of 1.5301, intercept of 1.1429, and correlation coefficient (r^2) of 0.9995. Sensitivity parameters revealed high detection capability with a limit of detection (LOD) of 6.46 ng mL^{-1} and limit of quantification (LOQ) of 19.38 ng mL^{-1}, calculated using the standard deviation of the blank and slope of the calibration

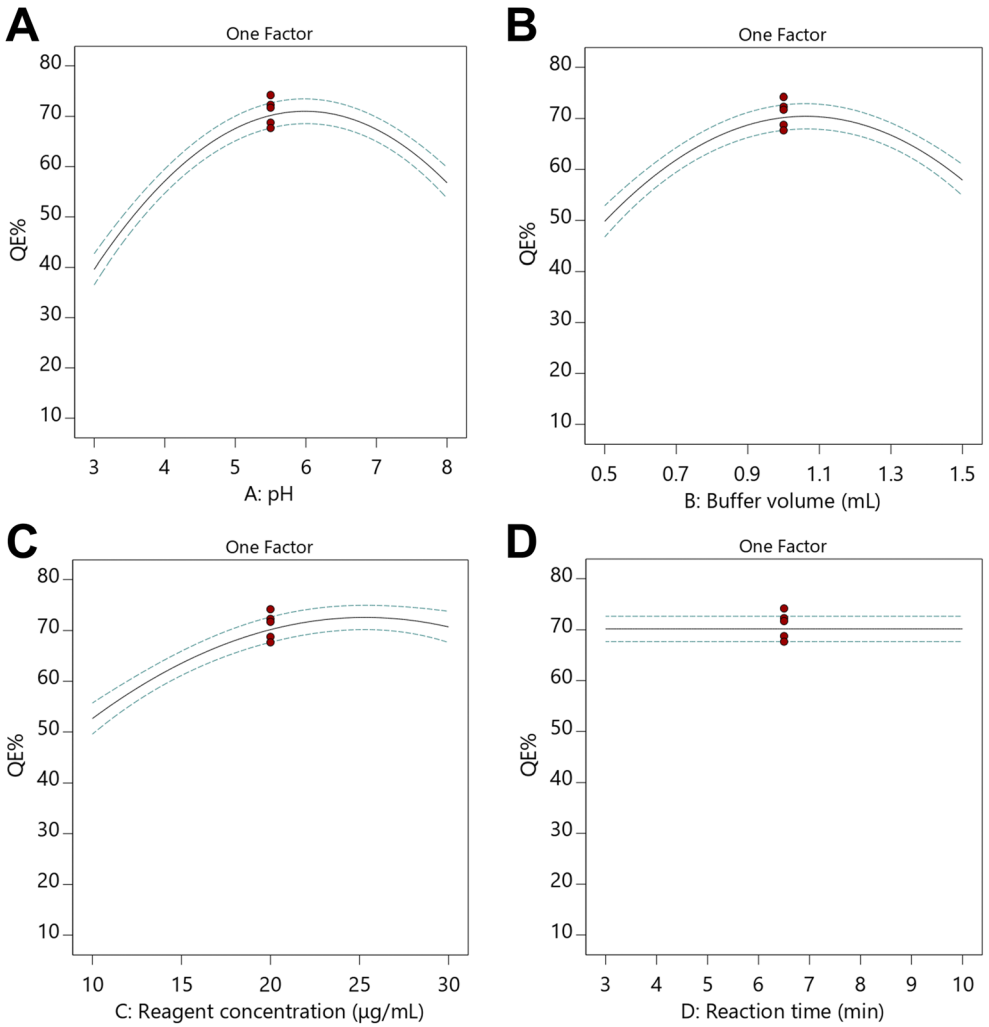

Fig. 4 Individual factor effects on fluorescence quenching efficiency (QE%) from Box–Behnken design, with all other factors at central values: (A) effect of pH (3.0–8.0) showing bell-shaped response with optimum at pH 5.6, consistent with complete erythrosin B deprotonation ($pK_a \approx 3.8$, 4.6) and preserved ivabradine cationic character ($pK_a \approx 9.3$); (B) effect of buffer volume (0.5–1.5 mL) with optimum at 1.1 mL; (C) effect of erythrosin B concentration (10–30 µg mL^{-1}) showing plateau above 25 µg mL^{-1} indicating binding site saturation; (D) effect of reaction time (3.0–10.0 min) showing flat response confirming rapid equilibrium formation. Dashed lines represent 95% confidence intervals derived from the quadratic model.

curve. These sensitivity parameters represent significant improvements over conventional HPLC-UV methods reporting detection limits in the 330–1190 ng mL^{-1} range, and are competitive with reported spectrofluorimetric methods for ivabradine, while offering the additional advantage of visible-region excitation at 528 nm that minimizes matrix autofluorescence interference commonly encountered with UV excitation-based fluorescence methods.

Selectivity was rigorously evaluated by testing the method's response to various potentially interfering substances commonly found in pharmaceutical formulations and biological matrices at 10 µg mL^{-1} concentration (10-fold excess) compared to 1 µg mL^{-1} ivabradine. As demonstrated in Fig. S5, ivabradine exhibited the highest quenching efficiency (~62%), while potential interferents including excipients, electrolytes, and biological components (tryptophan, tyrosine, glucose) showed minimal interference with quenching efficiencies below 5% even at this significant excess. Although the method demonstrated high selectivity under the tested conditions, fluorescent probes such as erythrosin B inherently suffer from non-specific binding interactions, unlike LC-MS/MS methods where structural confirmation is acquired through mass spectral fragmentation patterns. This limitation is evidenced in the literature where various drugs have been reported to interact with erythrosin B through different binding mechanisms. However, this limitation could be overcome using targeted extraction techniques such as molecularly imprinted polymers (MIPs) that provide molecular recognition specificity, or solid-phase extraction protocols designed to eliminate structurally similar interferents prior to fluorescence analysis.

Accuracy was evaluated through recovery studies at three concentration levels (0.05, 1.0, and 1.5 µg mL^{-1}) with three replicates at each level ($n = 9$ total determinations), yielding an overall accuracy of 99.77 ± 1.008% recovery (Table 4). Precision

Table 4 Comprehensive method validation parameters according to ICH Q2(R2) guidelines

Parameters		Ivabradine
Excitation wavelength (nm)		528
Emission wavelength (nm)		555
Linearity range (μg mL^{-1})		0.02–2.0
Slope		1.5301
Intercept		1.1429
Correlation coefficient (r^2)		0.9995
LOD (ng mL^{-1})		6.46
LOQ (ng mL^{-1})		19.38
Accuracy (%R) [a]		99.77 ± 1.008
Repeatability precision (%RSD) [b]		1.011
Intermediate precision (%RSD) [c]		1.851
Robustness (%R)	pH	98.67 ± 0.886
	Reagent conc.	100.65 ± 1.665
	Buffer volume	98.22 ± 0.750

[a] Average of 9 determinations (3 concentrations repeated 3 times). [b] % RSD of 9 determinations (3 concentrations repeated 3 times) measured on the same day. [c] % RSD of 9 determinations (3 concentrations repeated 3 times) measured in the three consecutive days.

was assessed at two levels: repeatability (intra-day precision) was determined from nine measurements across three concentration levels on the same day (%RSD = 1.011%), while intermediate precision was evaluated from nine measurements across three concentration levels repeated on three consecutive days (%RSD = 1.851%), both well below the ICH acceptance criterion of 2%. Robustness testing was performed in triplicate (n = 3) for each parameter variation, evaluating the method's resilience to deliberate variations in critical parameters including pH (±0.2 units), reagent concentration (±2 μg mL^{-1}), and buffer volume (±0.1 mL). The results showed minimal impact on analytical performance, with recovery percentages of 98.67 ± 0.886%, 100.65 ± 1.665%, and 98.22 ± 0.750% respectively, confirming method reliability during routine analysis despite minor experimental fluctuations (Table 4). The comprehensive validation study demonstrates that the developed method meets all ICH requirements for analytical procedures and is suitable for accurate and precise quantification of ivabradine in pharmaceutical and biological applications.

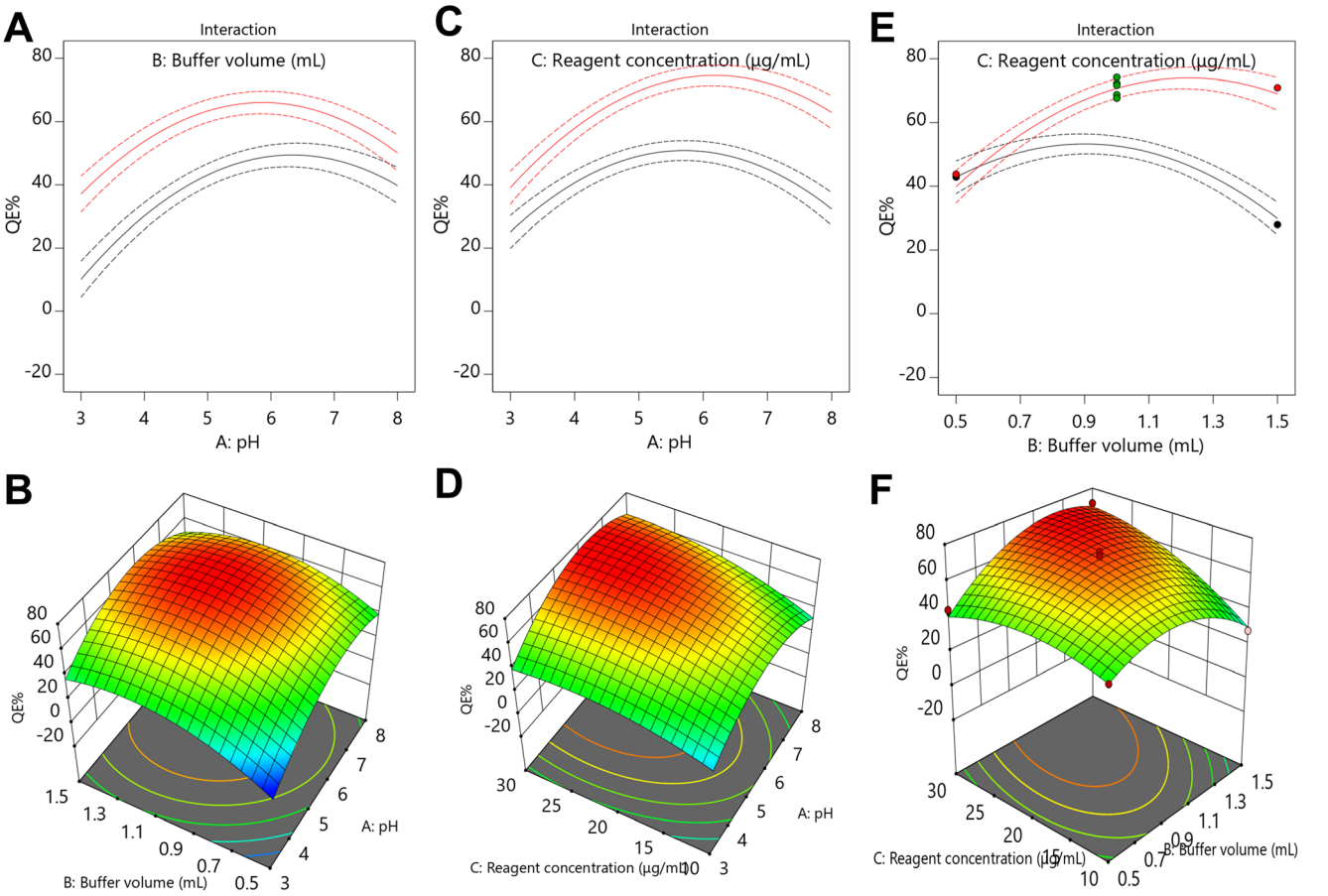

Fig. 5 Factor interaction plots and response surface analysis from Box–Behnken optimization (R^2 = 0.9727, F = 75.22, p < 0.0001): (A) two-dimensional interaction plot between pH and buffer volume showing moderate curvature; (B) three-dimensional response surface for pH-buffer volume interaction displaying broad optimal region; (C) pH-reagent concentration interaction plot exhibiting pronounced curvature; (D) three-dimensional surface for pH-reagent concentration interaction revealing distinct maximum at intermediate pH and higher concentrations; (E) buffer volume-reagent concentration interaction showing strong synergistic effects; (F) three-dimensional surface for buffer volume-reagent concentration displaying sharp maximum confirming significant interaction coefficient.

Table 5 Statistical comparison between the developed method and reported HPLC method for pharmaceutical analysis

Method	Mean[a]	SD	t-Test[b] (2.306)	P value	F-value[b] (6.338)	P value	θ_L[c]	θ_U[c]
Developed method	99.86	1.168	0.411	0.692	1.302	0.804	−1.888	1.317
Reported method	100.15	1.024						

[a] Average of five determinations. [b] The values in parenthesis are tabulated values of "t "and "F" at ($P = 0.05$). [c] Bias of ± 2% is acceptable.

3.6 Application to real samples

The validated method was successfully applied to the analysis of ivabradine in pharmaceutical formulations and biological matrices to demonstrate its practical applicability and reliability under real-world conditions. Commercial Procoralan 5 mg tablets were analyzed using the optimized procedure, and the results were statistically compared with a reported HPLC method to assess method equivalence.[14] The pharmaceutical analysis yielded satisfactory results with good agreement between the developed fluorescence method and the reference technique. Statistical evaluation presented in Table 5 demonstrated no significant differences between the two methods, with the developed method showing a mean recovery of 99.86% compared to 100.15% for the reported method. The calculated t-test value (0.411) was below the critical value (2.306) at 95% confidence level, indicating no significant bias between the methods. Similarly, the F-test value (1.302) was less than the critical value (6.338), confirming comparable precision between the techniques. The bias assessment using acceptance limits ($\theta_L = -1.888$ and $\theta_U = 1.317$) fell within the acceptable range of ±2%, further validating method equivalence and demonstrating that the developed method can serve as a reliable alternative to established chromatographic techniques for pharmaceutical quality control applications. Beyond analytical equivalence, the developed method offers clear practical advantages over the reference HPLC method[14] in terms of operational simplicity, requiring no expensive chromatographic columns, organic mobile phases, or lengthy equilibration times, thereby reducing both per-analysis cost and technical complexity for routine pharmaceutical quality control implementation.

Biological sample analysis was conducted using spiked human plasma samples at four concentration levels (0.025, 0.05, 1.0, and 1.5 μg mL^{-1}) to evaluate method performance in complex biological matrices. These concentrations encompass the reported therapeutic peak plasma concentrations (C_{max}) of ivabradine in humans, which range from approximately 9–42 ng mL^{-1} following single and repeated oral doses of 2.5–10 mg,[40] confirming that the lower spiked concentrations of 0.025 and 0.05 μg mL^{-1} are clinically relevant for therapeutic drug monitoring, while the higher concentrations of 1.0 and 1.5 μg mL^{-1} extend the method's applicability to pharmacokinetic studies and potential overdose monitoring situations. Recovery studies summarized in Table S3 demonstrated excellent extraction efficiency and minimal matrix effects, with recovery percentages ranging from 101.34% to 104.59% across all tested concentration levels. The relative standard deviation values remained below 5% for all concentrations, with the lowest RSD of 1.56% observed at the highest concentration level (1.5 μg mL^{-1}) and slightly higher variability at lower concentrations, which is typical for trace-level analysis in biological samples. The successful application to both pharmaceutical formulations and biological matrices confirms the method's versatility and suitability for diverse analytical applications, including pharmaceutical quality control, bioanalytical studies, and therapeutic drug monitoring programs.

3.7 Green analytical chemistry assessment

The environmental impact and sustainability of the developed erythrosin B-based fluorescence quenching method for ivabradine determination were comprehensively evaluated using three complementary assessment tools: AGREE,[41] BAGI,[42] and whiteness assessment using the RGB12 metrics.[43] This multi-dimensional evaluation approach provides a holistic assessment of the method's environmental friendliness, analytical practicality, and overall sustainability, addressing the growing demand for eco-conscious analytical procedures in pharmaceutical analysis.

The AGREE assessment (Fig. 6A) yielded an overall score of 0.76, indicating good greenness performance with several environmentally favorable characteristics. The circular pictogram reveals the method's strengths and areas for potential improvement across twelve evaluation criteria. The method achieved excellent scores (green segments) for the majority of criteria including sample preparation stages (4), derivatization (6), waste generation (7), analysis throughput (8), energy consumption (9), source of reagents (10), toxicity (11), and operator safety (12). These high scores reflect the method's minimal sample preparation requirements, absence of derivatization steps, reduced organic solvent consumption, good analytical throughput, low energy requirements due to ambient temperature operation, use of commercially available reagents, minimal toxicity concerns, and enhanced safety profile compared to chromatographic methods requiring hazardous mobile phases. However, the assessment identified areas requiring improvement, with sampling procedure (1) and automation/miniaturization (5) receiving moderate scores (yellow segments), indicating the need for further optimization and potential for method automation. Most notably, device positioning (3) received a lower score (red segment), suggesting that the fluorescence instrumentation requirements may limit accessibility compared to simpler analytical techniques, representing the primary area for sustainable method development.

The BAGI evaluation (Fig. 6B) provided a comprehensive assessment of analytical practicality, yielding an overall score of 77.5, which represents good analytical applicability. The star-

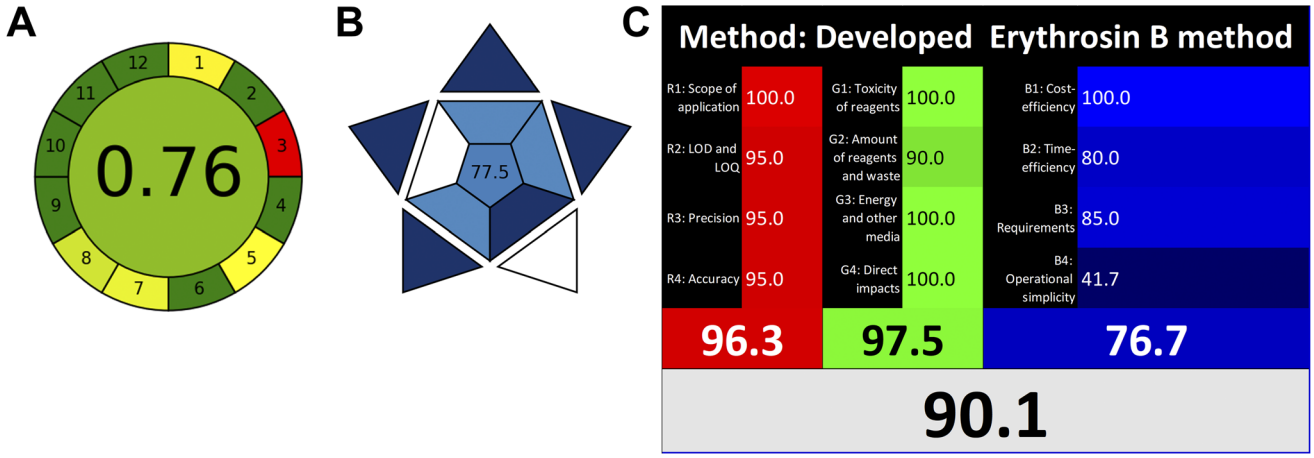

Fig. 6 Green analytical chemistry assessment of the developed method: (A) AGREE pictogram (overall score = 0.76) showing excellent performance for waste generation, energy consumption, reagent toxicity, and operator safety, with instrumentation accessibility identified as the primary area for improvement; (B) BAGI star diagram (overall score = 77.5) confirming method suitability for routine implementation through simple instrumentation, minimal sample preparation, and low reagent costs; (C) RGB12 whiteness assessment (overall score = 90.1) with dimensional scores of 96.3 (analytical), 97.5 (environmental), and 76.7 (economic), confirming excellent balance between analytical performance, environmental friendliness, and economic viability.

shaped pictogram illustrates the method's performance across ten practical criteria essential for routine analytical implementation. The assessment demonstrated that the method utilizes simple instrumentation readily available in most analytical laboratories, requires minimal sample preparation with low-cost reagents, and operates without the need for preconcentration steps. The evaluation confirmed that common commercially available reagents are employed, manual treatment and analysis are feasible, and the method can process an adequate number of samples per hour for routine applications. The bioanalytical sample volume requirements fall within acceptable ranges for practical implementation, further supporting the method's applicability in both pharmaceutical quality control and clinical analysis settings.

The RGB12 assessment (Fig. 6C) provided a detailed evaluation across three fundamental dimensions of analytical method sustainability: red (analytical), green (environmental), and blue (economic) aspects. The method achieved an overall whiteness score of 90.1, indicating excellent overall performance. The red dimension scored 96.3, reflecting superior analytical performance with high scores for scope of application, detection limits and quantification capabilities, precision, and accuracy. The green dimension scored 97.5, demonstrating high environmental friendliness through minimal toxicity of reagents, reduced amount of reagents and waste generation, low energy and media consumption, and negligible direct environmental impacts. The blue dimension scored 76.7, indicating good economic performance with excellent cost efficiency and reasonable time efficiency, though operational simplicity and analytical requirements showed moderate scores, suggesting areas where method automation could enhance economic attractiveness.

The comprehensive sustainability assessment demonstrates that the developed method represents a significant advancement in green analytical chemistry for pharmaceutical analysis. The high scores across all three assessment tools confirm that the method successfully balances analytical performance with environmental responsibility and economic viability. The minimal use of organic solvents, elimination of toxic mobile phases, reduced waste generation, and lower energy consumption compared to conventional chromatographic methods position this approach as an environmentally sustainable alternative for ivabradine determination. The assessment results support the method's potential for widespread adoption in pharmaceutical quality control laboratories seeking to implement greener analytical practices while maintaining analytical excellence and regulatory compliance. The achieved AGREE score of 0.76 and whiteness score of 90.1 are notably superior to those typically reported for HPLC-based methods for ivabradine determination,[11–14] which score poorly on waste generation and toxic solvent consumption criteria, further reinforcing the environmental and economic case for adopting fluorescence-based approaches in routine pharmaceutical analysis.

4 Conclusions

This study successfully developed and validated a novel, sensitive, and environmentally sustainable spectrofluorimetric method for ivabradine determination based on the fluorescence quenching of erythrosin B. The comprehensive investigation demonstrated that the method operates through a static quenching mechanism involving the formation of a stable 1 : 1 ground-state complex between the anionic erythrosin B probe and cationic ivabradine, as confirmed by Stern–Volmer analysis, thermodynamic studies, and Job's method. The negative thermodynamic parameters ($\Delta G = -35.49$ kJ mol^{-1}, $\Delta H = -24.54$ kJ mol^{-1}) indicated spontaneous, exothermic complex

formation driven by favorable electrostatic interactions, while quantum mechanical calculations using PM3 methodology provided molecular-level insights into the binding mechanism through multiple interaction sites. Box–Behnken experimental design optimization yielded optimal conditions (pH 5.6, buffer volume 1.1 mL, erythrosin B concentration 25 μg mL^{-1}, reaction time 4.0 minutes) that maximize analytical performance while ensuring practical implementation. The method demonstrated high analytical performance with excellent linearity (r^2 = 0.9995) over the range 0.02–2.0 μg mL^{-1}, superior sensitivity (LOD = 6.46 ng mL^{-1}, LOQ = 19.38 ng mL^{-1}), high accuracy (99.77 ± 1.008%), and precision (%RSD < 2%) that fully comply with ICH Q2(R2) guidelines. Successful application to pharmaceutical formulations and spiked human plasma samples confirmed the method's practical utility for both quality control and bioanalytical applications. The comprehensive green chemistry assessment using AGREE (0.76), BAGI (77.5), and whiteness (90.1) tools demonstrated excellent environmental sustainability, analytical practicality, and overall method sustainability, positioning this approach as a superior alternative to conventional chromatographic methods that require hazardous organic solvents and generate significant chemical waste.

Despite the method's numerous advantages, certain limitations warrant consideration for future development. The primary limitation concerns selectivity challenges inherent to fluorescence-based methods, where structurally similar compounds or matrix components with comparable binding affinities could potentially interfere with accurate quantification, unlike LC-MS/MS techniques that provide structural confirmation through mass spectral fragmentation. Additionally, the method's dependence on specific pH conditions and ionic strength requirements may limit its direct applicability to highly complex biological matrices without prior sample treatment. Future research should focus on enhancing selectivity through the development of molecularly imprinted polymer (MIP) extraction protocols that provide molecular recognition specificity for ivabradine, effectively eliminating potential interferents before fluorescence analysis. Integration of advanced sample preparation techniques such as solid-phase microextraction (SPME) or magnetic solid-phase extraction using functionalized nanoparticles could further improve method selectivity and sensitivity while maintaining environmental sustainability. Method automation through flow injection analysis (FIA) or microfluidic platforms would enhance throughput, reduce operator intervention, and improve reproducibility, addressing the economic dimension limitations identified in the whiteness assessment. Furthermore, expanding the method's scope through the development of multiplexed detection systems for simultaneous determination of ivabradine and its metabolites or co-administered cardiovascular drugs would increase its clinical utility and cost-effectiveness for therapeutic drug monitoring applications.

Conflicts of interest

There are no conflicts of interest to declare.

Data availability

The authors confirm that the data supporting the findings of this study are available within the article and its supplementary information (SI). Any additional data are available from the corresponding author upon reasonable request. Supplementary information is available. See DOI: https://doi.org/10.1039/d6ra00744a.

Acknowledgements

This work was supported and funded by the Deanship of Scientific Research at Imam Mohammad Ibn Saud Islamic University (IMSIU) (grant number IMSIU-DDRSP2602).

References

1 J. S. Koruth, A. Lala, S. Pinney, V. Y. Reddy and S. R. Dukkipati, *J. Am. Coll. Cardiol.*, 2017, **70**, 1777–1784.
2 L. Simon, B. Ghaleh, L. Puybasset, J.-F. Giudicelli and A. Berdeaux, *J. Pharmacol. Exp. Therapeut.*, 1995, **275**, 659–666.
3 J.-P. Vilaine, J.-P. Bidouard, L. Lesage, H. Reure and J.-L. Péglion, *J. Cardiovasc. Pharmacol.*, 2003, **42**, 688–696.
4 K. Fox, I. Ford, P. G. Steg, J.-C. Tardif, M. Tendera and R. Ferrari, *Eur. Heart J.*, 2015, **36**, 3291–3296.
5 R. I. Martin, O. Pogoryelova, M. S. Koref, J. P. Bourke, M. D. Teare and B. D. Keavney, *Heart*, 2014, **100**, 1506–1510.
6 K. Swedberg, M. Komajda, M. Böhm, J. S. Borer, I. Ford, A. Dubost-Brama, G. Lerebours and L. Tavazzi, *Lancet*, 2010, **376**, 875–885.
7 M. Böhm, K. Swedberg, M. Komajda, J. S. Borer, I. Ford, A. Dubost-Brama, G. Lerebours and L. Tavazzi, *Lancet*, 2010, **376**, 886–894.
8 J. S. Borer, K. Fox, P. Jaillon and G. Lerebours, *Circulation*, 2003, **107**, 817–823.
9 J.-C. Tardif, I. Ford, M. Tendera, M. G. Bourassa and K. Fox, *Eur. Heart J.*, 2005, **26**, 2529–2536.
10 W. Ruzyllo, M. Tendera, I. Ford and K. M. Fox, *Drugs*, 2007, **67**, 393–405.
11 E. A. Rashad, S. S. Elsayed, J. J. M. Nasr and F. A. Ibrahim, *Sustain. Chem. Pharm.*, 2024, **38**, 101476.
12 S. B. Kanthale, S. S. Thonte and D. K. Mahapatra, *J. Appl. Pharmaceut. Sci.*, 2019, **9**, 137–144.
13 B. Gülşen and S. E. Toker, *Anal. Methods*, 2025, **17**, 1111–1124.
14 J. Nowakowska, P. Pikul, M. Marszałł and K. Ciura, *J. Chem.*, 2017, **2017**, 2069571.
15 M. M. Eswarudu, A. L. Rao and K. Vijay, *J. Pharmacol. Toxicol. Methods*, 2022, **116**, 107186.
16 J. Jiang, L. Tian, Y. Huang and Y. Li, *Biomed. Chromatogr.*, 2013, **27**, 1603–1608.
17 C. Lu, Y. Jia, J. Yang, X. Jin, Y. Song, W. Liu, Y. Ding, X. Sun and A. Wen, *Acta Pharm. Sin. B*, 2012, **2**, 205–212.
18 A. A. Zoerner, C. Schroeder, A. A. Kayacelebi, M. T. Suchy, F.-M. Gutzki, D. O. Stichtenoth, J. Tank, J. Jordan and D. Tsikas, *J. Chromatogr. B*, 2013, **927**, 105–111.

19 N. F. Abo-Talib, M. H. Tammam and A. K. Attia, *RSC Adv.*, 2015, **5**, 95592–95597.
20 F. M. Abdel-Haleem, M. S. Rizk and M. M. El-Beshlawy, *RSC Adv.*, 2022, **12**, 17645–17654.
21 R. M. Alnemari, R. M. Alzhrani, M. H. Abduljabbar, F. M. Almutairi, M. M. Aldhafeeri, M. Almaghrabi, Y. S. Althobaiti, A. H. Almalki, M. A. Abdel Rahman and A. Serag, *Anal. Methods*, 2025, **17**, 5259–5268.
22 A. Serag, F. M. Almutairi, M. M. Aldhafeeri, R. M. Alzhrani, M. H. Abduljabbar, R. M. Alnemari, Y. S. Althobaiti and A. H. Almalki, *RSC Adv.*, 2025, **15**, 19468–19479.
23 A. Serag, R. M. Alnemari, M. H. Abduljabbar, M. E. Alosaimi and A. H. Almalki, *Spectrochim. Acta, Part A*, 2024, **315**, 124245.
24 F. M. Almutairi, Y. S. Althobaiti, M. H. Abduljabbar, R. M. Alzhrani, R. M. Alnemari, M. M. Aldhafeeri, A. Serag and A. H. Almalki, *Spectrochim. Acta, Part A*, 2025, **335**, 126000.
25 A. Serag, R. M. Alzhrani, R. M. Alnemari, M. H. Abduljabbar and A. H. Almalki, *Microchem. J.*, 2025, **215**, 114515.
26 P. M. Tailor and K. Naik, *Spectrochim. Acta, Part A*, 2022, **264**, 120330.
27 E. A. Rashad, S. S. Elsayed, J. J. M. Nasr and F. A. Ibrahim, *Spectrochim. Acta, Part A*, 2023, **289**, 122074.
28 S. M. Abo Elkheir, A. M. Zeid, J. J. M. Nasr and M. I. Walash, *Luminescence*, 2022, **37**, 1657–1665.
29 R. Aboshabana, A. M. Zeid and F. A. Ibrahim, *Spectrochim. Acta, Part A*, 2023, **295**, 122626.
30 M. H. Abduljabbar, M. M. Althobaiti, F. M. Almutairi, M. M. Aldhafeeri, M. F. Aldawsari, Y. S. Althobaiti, A. Serag and A. H. Almalki, *J. Photochem. Photobiol., A*, 2025, **466**, 116400.
31 R. A. Felemban, M. A. Algarni, A. A. Abd Al Maksoud, A. Alharbi, A. K. Bamaga, M. S. Alzahrani, A. I. Alzarea, A. Serag and A. H. Almalki, *Microchem. J.*, 2025, **216**, 114560.
32 Y. S. Alqahtani, A. M. Mahmoud and M. M. El-Wekil, *Talanta*, 2023, **253**, 124024.
33 A. Serag, A. H. Abdelazim, S. Ramzy, R. M. Alnemari, R. M. Alzhrani, M. H. Abduljabbar, Y. S. Althobaiti, M. E. Alosaimi, S. I. Alaqel and A. H. Almalki, *Talanta*, 2026, **296**, 128442.
34 M. Madhu, S. Santhoshkumar, W.-B. Tseng and W.-L. Tseng, *Front. Anal. Sci.*, 2023, **3**, 1258558.
35 R. A. Felemban, M. H. Abduljabbar, R. M. Alnemari, R. M. Alzhrani, Y. S. Althobaiti, M. F. Aldawsari, A. Serag and A. H. Almalki, *Anal. Methods*, 2025, **17**, 4334–4343.
36 M. E. El Sharkasy, M. M. Tolba, F. Belal, M. I. Walash and R. AboShabana, *Luminescence*, 2023, **38**, 2073–2085.
37 H. A. Elhamdy, M. Oraby, S. M. Derayea and K. M. Badr El-Din, *Luminescence*, 2024, **39**, e4845.
38 I. Guideline, ICH, Geneva, Switzerland, 2022, 1.
39 N. Boens, W. Qin, N. Basarić, J. Hofkens, M. Ameloot, J. Pouget, J.-P. Lefevre, B. Valeur, E. Gratton and M. Vandeven, *Anal. Chem.*, 2007, **79**, 2137–2149.
40 H. Y. Choi, Y.-H. Noh, S.-H. Cho, J.-L. Ghim, S. Choe, U.-J. Kim, J. A. Jung, K.-S. Bae and H.-S. Lim, *Clin. Ther.*, 2013, **35**, 819–835.
41 F. Pena-Pereira, W. Wojnowski and M. Tobiszewski, *Anal. Chem.*, 2020, **92**, 10076–10082.
42 N. Manousi, W. Wojnowski, J. Płotka-Wasylka and V. Samanidou, *Green Chem.*, 2023, **25**, 7598–7604.
43 P. M. Nowak, R. Wietecha-Posłuszny and J. Pawliszyn, *TrAC, Trends Anal. Chem.*, 2021, **138**, 116223.